

DEPOLARIZED SnO₂-BASED GAS ANODES FOR ELECTROWINNING OF SILVER IN MOLTEN CHLORIDES

S. Xiao^{a,*}, G. M. Haarberg^b

^a Anhui University of Technology, School of Metallurgy and Resource, Maanshan, China

^b Norwegian University of Science and Technology, Department of Materials Science and Engineering, Trondheim, Norway

(Received 14 October 2012; accepted 28 January 2013)

Abstract

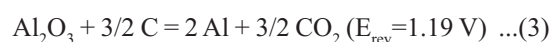
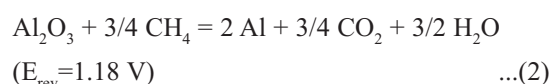
SnO₂-based porous anodes were prepared and the behavior of gas bubbles on the porous anodes with different original coarse grain size, immersed in ethanol to simulate molten chlorides, was primarily investigated. SnO₂-based porous anodes were used as gas anodes for the electrowinning of silver in CaCl₂-NaCl-CaO-AgCl melts at 680 °C. Hydrogen was introduced to the anode/electrolyte interface through the gas anode. Carbon was used as the cathode. Obvious depolarization of the anode potential was observed after the introduction of hydrogen comparing with no reducing gas introduced, indicating the involvement of hydrogen in the anode reaction. Metallic silver was deposited on the cathode.

Keywords: SnO₂-based gas anodes; Depolarization; Silver deposition; Hydrogen oxidation

1. Introduction

Aluminum and its alloy have excellent physical and chemical properties and are widely used in different areas such as transportation, construction and packaging. Aluminum is produced via Hall-Héroult process. In this process consumable carbon anodes made from petroleum coke are used in the electrowinning of aluminum from dissolved Al₂O₃ in molten cryolite. The disadvantages of using the consumable carbon anodes are the release of the greenhouse gas CO₂ and complicated operations of periodic adjustment and replacement of the anodes. Thus inert anodes of metals, ceramics or cermets have been studied as alternative for the consumable carbon anodes since they reduce the CO₂ emission significantly and are not consumable. However, inert oxygen evolving anodes require a higher anode potential than carbon, resulting in higher demand for expensive electrical power. An alternative approach is to substitute the consumable carbon anode with a reducing gas anode (e.g. H₂ and CH₄), resulting in a reduction in CO₂ emission and, theoretically, the same requirement of electrical power as that for carbon anode, while at the same time avoiding the periodic adjustment and replacement of the carbon anode. A reducing gas anode is a porous anode with the introduction of reducing gases and the anode reaction involves the oxidation of the reducing gases.

For comparison, the overall reactions for electrowinning of aluminum from its oxide using inert, natural gas, and consumable carbon anodes at 960 °C are given in Equations (1) to (3), respectively.



The theoretical cell voltage is about the same for the carbon and the natural gas anode at 960 °C, while a higher cell voltage is required for an oxygen producing anode.

Investigations of introducing reducing gases to the porous anodes for electrowinning in molten salts have been reported before. Porous carbon was mainly used as the anode and a small depolarization effect was observed in molten cryolite for aluminum production [1-4]. In a US patent from 2000 a non-consumable anode of the type used for solid oxide fuel cells (SOFC) supplied with reformed natural gas was published for the electrowinning of aluminum [5]. Later, several papers [6-8] reported the solid oxide membrane technology for producing metals from their oxides in molten salts, with the introduction of hydrogen. In 2000 in Canada a similar idea was

* Corresponding author: jxddroc@126.com

applied in magnesium production in molten chlorides resulting in the depolarization effect and the formation of HCl gas [9]. In addition a thermodynamic analysis considering carbon and nickel-based hydrogen diffusion anodes in the electrolyte ($\text{Na}_3\text{AlF}_6\text{-AlF}_3\text{-Al}_2\text{O}_3$) was carried out to identify optimum operating parameters in aluminum production in 2007 [10] and a nickel-based hydrogen diffusion anode was used and investigated in an experimental study of aluminum electro-winning, showing measurable depolarization of the anode potential in 2011 [11].

Carbon, nickel metal and solid oxide membrane coated with metal have been used as the gas anodes, showing the involvement of the anode itself into the anode reaction or corrosion of the anode materials. Actually, SnO_2 -based materials are proved to be good candidates due to their low solubility in molten cryolite and good electrical conductivity. In this paper, SnO_2 -based gas anodes with different original coarse grain size were studied in molten chlorides as the basis for future research on aluminum electrolysis in more corrosive molten cryolite, since they have been investigated in molten chlorides as an inert anode for FFC process showing good performance [12, 13]. $\text{CaCl}_2\text{-NaCl-CaO-AgCl}$ melts were chosen as the electrolyte since the deposition of silver is simple and the anode reaction of O^{2-} with reducing gas is analog to that in aluminum electrolysis. The authors have preliminarily demonstrated the depolarization effects of NiFe_2O_4 -based anodes, SnO_2 -based gas anodes and Pt in molten chlorides [14-17].

2. Experimental

Porous SnO_2 -based anodes were made from Stannex ELR blocks (Dyson Thermal Technologies). The preparation procedure and characterization are described in a previous publication [16]. The green body was a mixture of coarse grains with the particle size of 45-90 μm , 90-180 μm and 180-355 μm from Stannex ELR blocks and fine $\text{SnO}_2/\text{CuO}/\text{Sb}_2\text{O}_3$ powders, which was rammed inside mullite tubes and then sintered at 1300 $^\circ\text{C}$ for 3 hours. In the designed SnO_2 -based depolarized gas anode an inner steel tube for feeding gas was installed and surrounded concentrically by an outer steel tube with a bypass valve on the top, as shown in Figure 1. The gases were introduced from the inner tube, which made the gases pass through the porous anode and into the electrolyte when the valve is closed.

$\text{CaCl}_2\text{-NaCl}$ mixture was chosen as the basic melts with addition of CaO (Merck, 97%) and AgCl (VWR, Prolabo). CaCl_2 was prepared from $\text{CaCl}_2 \cdot 2\text{H}_2\text{O}$ (Merck, 99%) by drying at 200 $^\circ\text{C}$ in air for 48 hours. NaCl (Merck, 99.5%) and CaO were also dried at 200 $^\circ\text{C}$ in air to remove surface water. The composition of

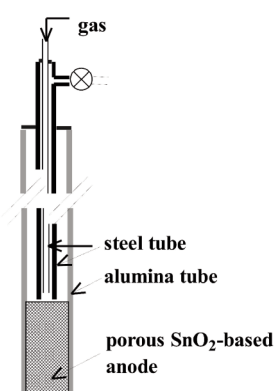


Figure 1. Schematic design of a SnO_2 -based gas anode.

the electrolyte is $\text{CaCl}_2\text{-NaCl}$ (70-30 mol%)-CaO (16 mol%)-AgCl (4.5 mol%). The schematic of the electrochemical cell is shown in Figure 2. The anode (working electrode) is simply shown here. A carbon cylinder was the cathode (counter electrode). The reference electrode was AgCl /Ag with 4 mol% AgCl in molten $\text{CaCl}_2\text{-NaCl}$ inside a mullite tube, a silver wire serving as the lead. All the potentials in molten chlorides were referred to AgCl/Ag reference electrode.

The whole electrochemical cell was placed in a vertical tube furnace, heated by resistance wires and connected to a temperature controller. The furnace was made gas tight to ensure an inert atmosphere inside it during the experiment. The electrochemical measurements of the system were carried out by an Autolab potentiostat (PGSTAT 30) operating with GPES software (General Purpose Electrochemical System), with an upper limit of 1 A.

3. Results and discussion

3.1 The behavior of bubbles on the porous anodes

Porous anodes with different coarse grain size were partly immersed in ethanol at room temperature with the introduction of argon to simulate the bubble behavior in molten chlorides, although these two solvents have different viscosity and interfacial tension. Argon with a flow rate of 10 $\text{cm}^3 \text{min}^{-1}$ was supplied to the porous anode with coarse grain size of 45-90 μm and the bubbles forming on the bottom was observed, shown in Figure 3 (a) and (b). Most of the gas came out from the bottom gap between porous SnO_2 and the mullite tube (a) (the big bubble in the middle not included, but to form the final large bubble) and a large bubble was formed immediately covering the entire anode bottom (b). After the large bubble burst, new bubbles grew repeatedly with a period of ~ 3 seconds. With an increase of the particle size to 90-180 μm , part of the gas came out from the

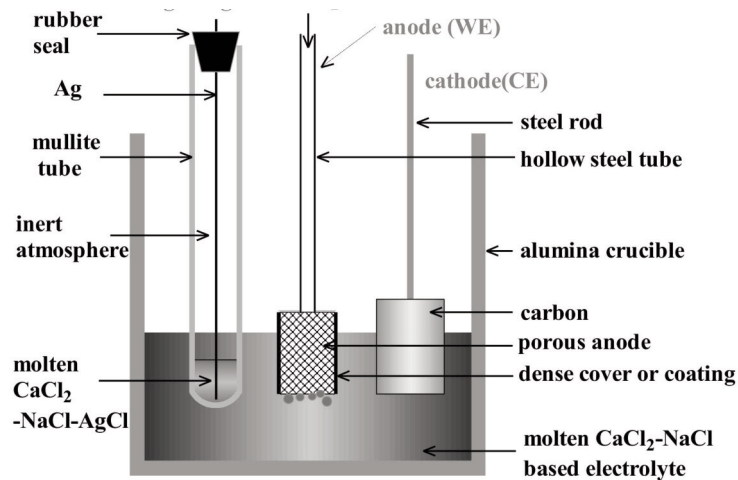


Figure 2. Schema of the electrochemical cell in molten chlorides.

bottom gap between porous SnO_2 and mullite tube and part of them from the bottom of the porous anode (c). These bubbles also accumulated and evolved into a large bubble covering most part of the bottom (d), with a period of ~ 2 seconds. By increasing to 180-355 mm, most of the gas came out from the bottom (e). Distributed small bubbles with a diameter of about 2 mm were formed and accumulated, evolving into a larger bubble almost covering the whole bottom (f), periodically every second.

With the increase of coarse grain size the shrinkage of the green body is decreasing after sintering. This led to smaller gap between the porous SnO_2 and the mullite tube. Simultaneously large coarse grain size resulted in large pores which facilitated the flow of gas. So it is easier for the gas to go through the porous anode from its bottom with the increase of the coarse grain size. The corresponding

period was also decreased.

3.2 Galvanostatic electrolysis

The applied current on the electrochemical cell was chosen as 0.4-0.6A to keep the anode potential < 0.8 V vs AgCl/Ag under the case of no hydrogen introduction, to avoid the evolution of chlorine and ensure the oxidation of oxide ion on the anode from a previous study [15]. Porous SnO_2 -based anode with coarse grain size of 45-90 mm was studied in molten CaCl_2 -NaCl (70-30 mol %)-CaO (16 mol %)-AgCl (4.5 mol %) at 680 °C. Constant current electrolysis was performed with an apparent current density of 0.04 A cm^{-2} and the response of the anode potential (a) and cell voltage (b) was shown in Figure 4. For $0 < t < 2400$ seconds, argon gas was introduced; the anode potential increased to ~ 0.7 V slowly and then became

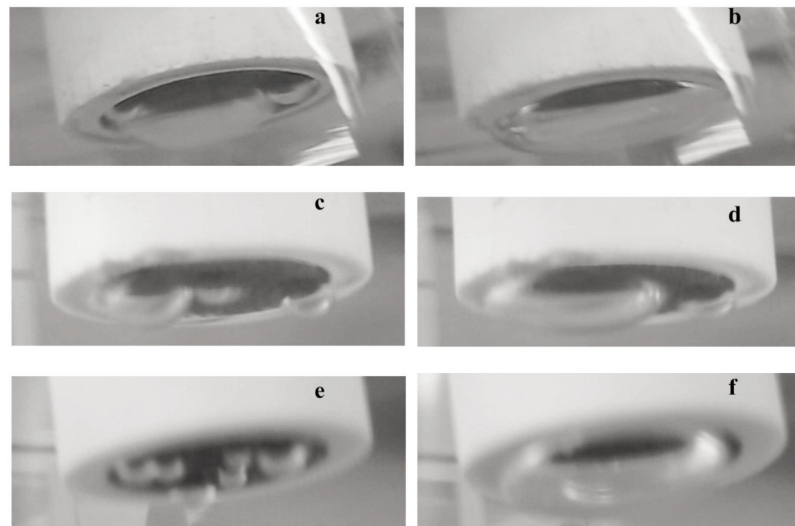


Figure 3. Photos of bubble behavior for SnO_2 -based gas anodes with different coarse grain size, (a) and (b), 45-90 mm, (c) and (d), 90-180 mm, (e) and (f), 180-355 mm.

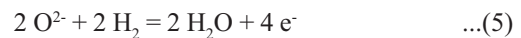
relatively stable with noise. During $2400 < t < 5400$ seconds, $10 \text{ cm}^3 \text{ min}^{-1}$ hydrogen was fed resulting in larger fluctuations on the anode potential with a period of ~ 1200 seconds and relatively stable anode potential and cell voltage. These periodic disturbances could be caused by periodic change of the surface area of the SnO_2 -based anode resulting in varying current density, which is responsible for the varying anode potential and cell voltage. For $5400 < t < 7500$ seconds, $20 \text{ cm}^3 \text{ min}^{-1}$ hydrogen was introduced; the anode potential exhibited smaller fluctuations with a shorter period of ~ 300 seconds and still relatively stable anode potential and cell voltage. For $7500 < t < 10500$ seconds, $30 \text{ cm}^3 \text{ min}^{-1}$ hydrogen was supplied; 900 seconds later the anode potential began to lower down. For $t > 10500$ seconds, argon was re-introduced and anode potential continued to maintain for 1500 seconds before returning to a higher level than the initial value. At the same time the cell voltage followed the same trend shown in Figure 4 (b). In this case no depolarization effect was found until the flow rate was increased to $30 \text{ cm}^3 \text{ min}^{-1}$. The decrease of anode potential and cell voltage was around 0.5 and 0.4 V, respectively, which was maintained for 3600 seconds.

An applied current of 0.04 A was chosen to keep

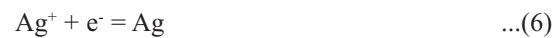
the anode potential $< 0.8 \text{ V}$ vs AgCl/Ag. During the first 2400 seconds, it was thought that oxygen was evolved at the anode according to reaction (4) from the previous study [15].



Introduction of hydrogen with a flow rate of $30 \text{ cm}^3 \text{ min}^{-1}$ to the anode led to decrease of the anode potential and cell voltage by about 0.5 and 0.4 V, respectively. The decrease was considered due to the hydrogen gas being involved in the anode reaction (reaction (5)).



At the same time, on the cathode silver was deposited according to reaction (6). The corresponding picture of the collected silver metal (dendrite) is shown in Figure 5.



Two porous SnO_2 -based anodes with coarse grain size of 90-180 and 180-355 μm were also investigated. Figure 6 (a) shows the anode potential dependency on time and gas species under constant current electrolysis at an apparent current density of 0.06 A cm^{-2} . Introducing $10 \text{ cm}^3 \text{ min}^{-1}$ hydrogen had

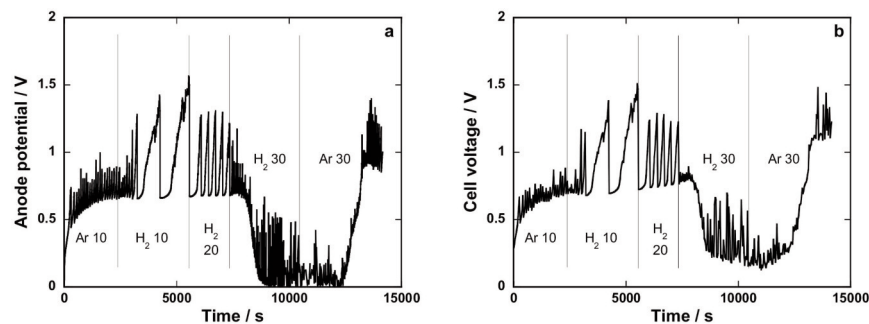


Figure 4. Anode potential (a) and cell voltage (b) versus time during constant current electrolysis (0.04 A ; apparent current density 0.04 A cm^{-2}) using a porous SnO_2 -based anode with coarse grain size of 45-90 μm in molten CaCl_2 - NaCl (70-30 mol%)- CaO (16 mol%)- AgCl (4.5 mol%) at $680 \text{ }^\circ\text{C}$. (Numbers in the figures are corresponding to the flow rate $\text{cm}^3 \text{ min}^{-1}$)

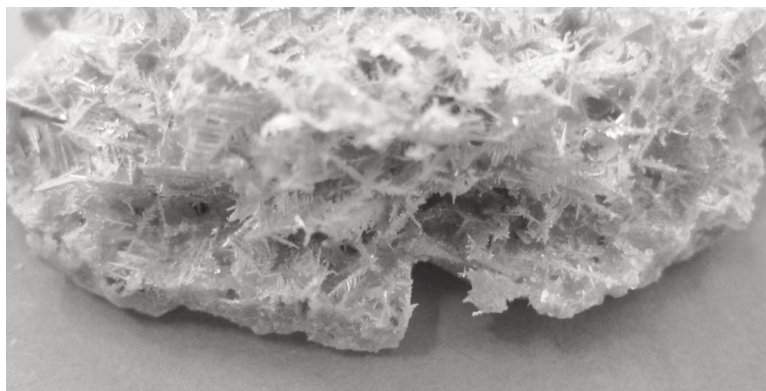


Figure 5. A photo of the deposited dendrite silver from the cathode.

no effect on the anode potential. When the flow rate was increased to $20 \text{ cm}^3 \text{ min}^{-1}$, a decrease of the anode potential of about 0.6 V was observed. At 10200 seconds argon was re-introduced; the low level continued to be maintaining for about 4800 seconds before growing to $\sim 0.7 \text{ V}$. Figure 6 (b) shows the anode potential versus time and gas species under constant current electrolysis at an apparent current density of 0.06 A cm^{-2} . In this case introduction of hydrogen ($10 \text{ cm}^3 \text{ min}^{-1}$) led to a decrease of the anode potential of around 0.5 V. The anode potential returned to a higher level during the introduction of hydrogen indicating that hydrogen did not depolarize the anode after around 4800 seconds depolarization.

From the results on the porous SnO_2 -based anodes with different coarse grain size, introduction of hydrogen caused a decrease of the anode potential of around 0.5 V. It was found that with the increase of the coarse grain size of the porous SnO_2 -based anode, more gas flowed out of the bottom of the anode, rather than escaping from the gap between SnO_2 and the mullite tube, and a lower flow rate of hydrogen was necessary to achieve the depolarization effect. For coarse grain size of 45-90, 90-180 and 180-355mm, the required flow rate of hydrogen is 30, 20, $10 \text{ cm}^3 \text{ min}^{-1}$, respectively. For anodes with smaller coarse grain size and finer pore size, more amount of gas might be required for forcing gas to go through the SnO_2 to build three-phase boundary for the anode reaction.

A summary of bubble behavior and needed flow rate to achieve the depolarization effect for the gas anodes with different coarse grain size was shown in Table 1.

4. Conclusions

SnO_2 -based gas anodes with coarse grain size of 45-90, 90-180 and 180-355mm in the green body were prepared. The behavior of the bubbles on the anodes was investigated when the anodes were immersed into liquid ethanol with the introduction of argon to simulate their behavior in the molten electrolyte. With the increase of the coarse grain size, more bubbles pass through the porous SnO_2 -based materials. Galvanostatic electrolysis was applied on the gas anode and the cathode. Decrease of anode potentials of around 0.5 V after introduction of hydrogen for the gas anodes with different coarse grain size was demonstrated. In addition, it was found that with the increase of the coarse grain size of the porous SnO_2 -based anode, a lower flow rate of hydrogen was necessary to achieve the depolarization effect. For coarse grain size of 45-90, 90-180 and 180-355mm, the required flow rate of hydrogen is 30, 20, $10 \text{ cm}^3 \text{ min}^{-1}$, respectively. On the cathode deposited dendrite silver metal was collected. The demonstration of depolarization effect of the gas anode in molten chlorides justifies its further investigation in more corrosive molten cryolite for aluminum electrolysis.

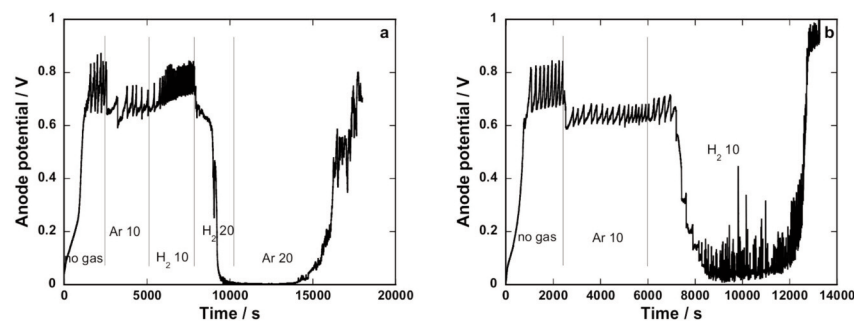


Figure 6. Anode potentials versus time during constant current electrolysis (0.06 A ; apparent current density 0.06 A cm^{-2}) using porous SnO_2 -based anodes with coarse grain size of 90-180 mm (a) and 180-355 mm (b) in molten CaCl_2 - NaCl (70-30 mol%)- CaO (16 mol%)- AgCl (4.5 mol%) at 680°C . (Numbers in the figures are corresponding to the flow rate $\text{cm}^3 \text{ min}^{-1}$)

Table 1. Bubble behavior and needed flow rate to achieve the depolarization effect for the gas anodes.

Coarse grain size of the porous anodes (mm)	Bubble channels	Growth period of large bubble (s)	Needed flow rate to achieve depolarization ($\text{cm}^3 \text{ min}^{-1}$)
45-90	Gap between mullite tube and porous SnO_2	3	30
90-180	Both from the gap and porous SnO_2	2	20
180-355	Porous SnO_2	1	10

Acknowledgement

The authors are grateful for the financial support from the GASSMAKS program of the Norwegian Research Council, Grant No. 182546/I30 and for valuable discussions with staff from SINTEF and Department of Materials Science and Engineering, NTNU. The authors are also grateful for the preparation of the anodes by Ove Paulsen and Tommy Mokkelbost from SINTEF.

References

- [1] M. L. Ferrand, Bulletin de la Societe Francaise des electriciens, 79 (1957) 412-413.
- [2] V. V. Stender, V. V. Trofimenko, Khim. Tekhnol., 12 (1969) 41-45.
- [3] M. L. Kronenberg, J. Electrochem. Soc., 116 (1969) 1160-1164.
- [4] J. Xue, A. P. Ratvik, Patent no. WO03102273, 2003.
- [5] R. A. Rapp, Patent no. US6039862, 2000.
- [6] U. B. Pal, D. E. Woolley, G. B. Kenney, JOM, 53 (2001) 32-35.
- [7] A. Krishnan, X. Lu, U. B. Pal, Metall. Mater. Trans. B, 36B (2005) 463-473.
- [8] U. B. Pal, A. C. Powell IV, JOM, 59 (2007) 44-49.
- [9] W. G. Van, Patent no. WO00/53826, 2000.
- [10] S. Namboothiri, M. P. Taylor, J. J. J. Chen, M. M. Hyland, M. A. Cooksey, Light Met. (2007) 379-384.
- [11] S. Namboothiri, M. P. Taylor, J. J. J. Chen, M. M. Hyland, M. A. Cooksey, Electrochim. Acta, 56 (2011) 3192-3202.
- [12] R. Barnett, K. T. Kilby, D. J. Fray, Metall. Mater. Trans. B, 40B (2009) 150-157.
- [13] K. T. Kilby, S. Q. Jiao, D. J. Fray, Electrochim. Acta, 55 (2010) 7126-7133.
- [14] S. Xiao, T. Mokkelbost, G. M. Haarberg, A. P. Ratvik, J. H. Kvello, K. S. Osen, H. M. Zhu, ECS Trans., 16 (2009) 583-588.
- [15] S. Xiao, T. Mokkelbost, G. M. Haarberg, A. P. Ratvik, H. Zhu, ECS Trans., 28 (2010) 361-366.
- [16] T. Mokkelbost, O. Paulsen, S. Xiao, G. M. Haarberg, A. P. Ratvik, ECS Trans., 28 (2010) 211-219.
- [17] G. M. Haarberg, E. Kvalheim, A. P. Ratvik, S. Xiao, T. Mokkelbost, Trans. Nonferrous Met. Soc. China, 20 (2010) 2152-2154.